Dielectric Properties of Fast Sol−Gel Glasses

Anna Gutina,[†] Yair Haruvy,[‡] Irith Gilath,[‡] Ekaterina Axelrod,[†] Nick Kozlovich,[†] and Yuri Feldman*,[†]

Department of Applied Physics, The Hebrew University of Jerusalem, Jerusalem 91904, Israel, and Division of Applied Radiation Technology, Soreq NRC, Yavne 81800, Israel

Received: January 4, 1999; In Final Form: April 19, 1999

The broad-band dielectric spectroscopy method was employed to investigate glasses of fine porosity produced via the fast sol−gel route. The study was carried out in the frequency range 20 Hz to 1 MHz and temperature interval −100 to +120 °C on the sol−gel glasses prepared at temperatures between 60 and 100 °C. The dielectric response data were analyzed both in frequency and time domains and interpreted in terms of the various non-Debye relaxation processes. A superposition of the Havriliak−Negami formula $\Delta\epsilon/[1 + (i\omega\tau)^{\alpha}]^{\beta}$ and Jonscher's term $(i\omega)^{(n-1)}$ was used for the fitting procedure and the quantitative analysis of the dielectric spectra. Here, $\Delta\epsilon$ is the dielectric strength and τ is the characteristic relaxation time. The parameters α and β describe the symmetric and asymmetric broadening of the relaxation process, and n is a Jonscher parameter for the high-frequency part of the relaxation process. It was shown that the complex dielectric behavior of the sol−gel glasses could be described in terms of several distributed dielectric relaxation processes and the dc conductivity part. At the low-temperature wing the strong relaxation process can be observed for all the samples. It can be attributed to the ion motion of the mobile molecules and ions anchored on the methoxy residual groups in the matrix. The second process is associated with percolation of excitation along the developed fractal structure of connected pores. The excitation is coursed by the movements of charge carriers within the pores. The dielectric relaxation response of this process in frequency and/or time domains can be used in order to calculate the porosity of the materials and fractal dimension of the porous space. The nature of the third process is different for various samples. It can be attributed to the fast mobility of the terminal oxygen groups and to the local mobility of the chain fragments located between neighboring knots of the entangled three-dimensional network.

1. Introduction

Noncrystalline solids, glass, and ceramics in particular are of special interest to the scientific community, being the core materials for a wide variety of new applications. The sol−gel reaction is a synthetic route by which metal alkoxide monomers, silane alkoxides in particular, are converted to ceramic/glassy materials by a sequence of hydrolysis and condensation reactions.[1] The hydrolysis stage (see eq 1) involves reaction with water, which is catalyzed by an acid or a base, and formation of alcohol.

$$\mathrm{Si(OR)_4} \xrightarrow{\mathrm{H_2O}} \mathrm{Si(OR)_3OH} \xrightarrow{\mathrm{H_2O}} \mathrm{Si(OR)_2(OH)_2} \xrightarrow{\mathrm{H_2O}} \mathrm{SiOR(OH)_3} \xrightarrow{\mathrm{H_2O}} \mathrm{Si(OH)_4} \quad (1)$$

The condensation stage (see eq 2) involves formation of M−O−M bonds and results in siloxane macromolecules and small condensates of water or alcohol.

$$\equiv\mathrm{SiOH} + \mathrm{HOSi}\equiv \xrightarrow{-\mathrm{H_2O}} \equiv\mathrm{Si{-}O{-}Si}\equiv; \quad \equiv\mathrm{SiOH} + \mathrm{ROSi}\equiv \xrightarrow{-\mathrm{ROH}} \equiv\mathrm{Si{-}O{-}Si}\equiv \quad (2)$$

The new fast sol−gel method recently introduced[2−5] enables facile preparation of siloxane-based glassy materials in which polymerization is completed within minutes and curing within a few hours. The fast sol−gel synthesis employs methyl-substituted alkoxysilane monomers and yields crack-free films as long as the *average* number of alkyl groups per silane equals, or is greater than, 1[2]:

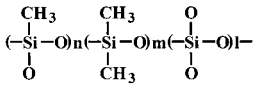

$$(n+2m)/(n+m+l) \geq 1 \quad (3)$$

Recently, the potential of cast-molding micro-optical arrays from the fast sol−gel-derived resins has been demonstrated.[6] This novel technique, which involves very low contraction of the siloxane matrix upon curing, even enables two-sided patterning of the sol−gel derived arrays having a few cm in diameter and more than 1 cm in thickness. All these features hint[2,6] that unlike most siloxane-derived glasses, the fast sol−gel derived glassy matrices comprise primarily polymer-like multiple-chain nanostructures rather than ceramic-like multiple-grain nanostructures.

Sol−gel methods have been extensively investigated for the fabrication of optical elements, both passive and active.[7] Encagement of relatively high concentrations of discrete guest molecules in these new glassy matrices, aimed at various aspects of nonlinear optics,[2,4,8] has also been demonstrated. These studies were followed by a comprehensive study of the chemical

* To whom correspondences should be addressed. Phone: +972-2-6586187. E-mail: Yurif@vms.huji.ac.il. Fax: +972-2-5663878.
[†] The Hebrew University of Jerusalem.
[‡] Soreq NRC.

10.1021/jp990008z CCC: $18.00
Published on Web 06/15/1999

and physical processes involved in curing of this glass and the consequent encaging of guest molecules.[9,10] Such matrices are of special interest for the encagement of chromophore molecules that facilitate the fabrication of optically active elements, nonlinear optical (NLO) ones in particular,[11,12] in which chromophore molecules of high NLO activity are discretely encaged in the matrix.

While sol−gel materials production, structural manipulation, and microarchitecture control undergo rapid progress,[6] their internal nanostructural features are vaguely understood. The lack of data on nanostructural details in such materials, both static and dynamic, which strongly affect their characteristics and performance, impedes further progress in controlling and manipulating their nanoarchitecture.

The dielectric response has been found to be very sensitive to the geometrical nano- and mesostructural features of the porous matrix and different materials filling the pores.[13] Dipole molecules or ions encaged in the pores perform a role of labels and provide a cooperative relaxation of the materials related to the interpore connection. Analysis of such dielectric response enables us to define the fine morphology and structural transitions in the porous systems. Thus, dielectric spectroscopy can furnish information on the dielectric permittivity of glass material, dc conductivity, and macroscopic dipole correlation functions. When these data are fit to the corresponding dynamic and morphological model, it is possible to infer some information about the geometry, fractal dimensions, mesostructural features, and the dynamics of pore-encaged molecules in the studied materials.

The purpose of the present study is to utilize the facile technique of dielectric spectroscopy measurements in order to decipher the nanostructural features of the fast sol−gel derived polymer-like glassy matrices. Special attention is conferred to two salient features of all glasses: the porosity, affecting the glass capacity to host, retain, and encage guest molecules; its fractality, affecting the glass−host relative motion.

2. Experimental Section

A. Preparation of Sol−Gel Samples. The sol−gel matrices to be investigated were made according to a standard protocol. All samples were made from a mixture of methyltrimethoxysilane (MTMS) and tetramethyl orthosilicate (TMOS) and catalyzed by 10^{-2} M HCl aqueous solution. The hydrolysis and polymerization were made employing the 85/15//19/1.5 recipe and the fast sol−gel route described in detail elsewhere.[6] The set of matrices for this study was prepared at sol−gel reaction temperatures of 100, 90, 80, 70, and 60 °C. Samples were cast in the form of flat round slabs, 40 mm in diameter and ∼1 mm thickness, following vacuum-assisted out-distillation to ∼48% of the original weight. No dopants have been added in this series. All the samples were cured for 150 h at 65 °C at ambient humidity and 16 h at ambient temperature and humidity, and they were then examined in the dielectric spectroscopy laboratory.

B. Dielectric Spectroscopy Measurements. Dielectric measurements in the frequency range 20 Hz to 1 MHz were performed by using a broad-band dielectric spectrometer BDS 4284 (NOVOCONTROL) with automatic temperature control by QUATRO Cryosystem in the range −100 to +120 °C. The accuracy of the measured dielectric permittivity and losses is better than 3%.[14] The measurements were carried out in the following way. Each of the samples was placed in the sample cell at room temperature, and the measurements were then performed by cooling the samples from 20 °C to −100 °C . The samples were then measured at intervals of 5 °C upon heating them from −100 to 120 °C.

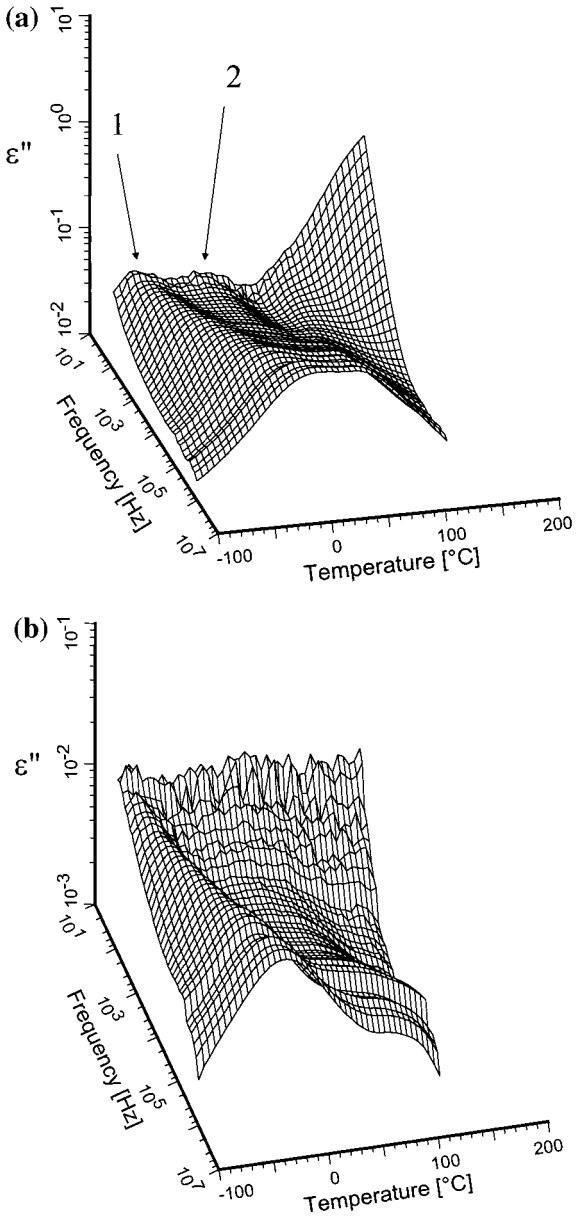

Figure 1. Three-dimensional plots of the frequency and temperature dependence of the dielectric losses for the fast sol−gel derived matrices at 100 °C (a) and 60 °C (b).

For a quantitative analysis of the dielectric spectra for all the relaxation processes a superposition of the Havriliak−Negami (HN) formula $\Delta\epsilon_j/[1 + (i\omega\tau_j)^{\alpha_j}]^{\beta_j}$ and Jonscher's empirical term $(i\omega)^{n_j-1}$ has been fitted to the isothermal data of the complex dielectric permittivity[13] $\epsilon^*(\omega)$. Here, $\Delta\epsilon_j$ is the dielectric strength and τ_j the mean relaxation time. The index j refers to the different processes that contribute to the dielectric response. The parameters α_j and β_j describe the symmetric and asymmetric broadening of the relaxation process; n_j is a Jonscher parameter for the high-frequency part of the respect relaxation process. In the case of the relaxation process including a contribution of electrical conductivity, the superposition of the HN function and the conductivity term was used.

3. Results and Discussion

All the samples are denoted herein by the temperature at which their sol−gel reactions took place, e.g., 100, 90, etc. A

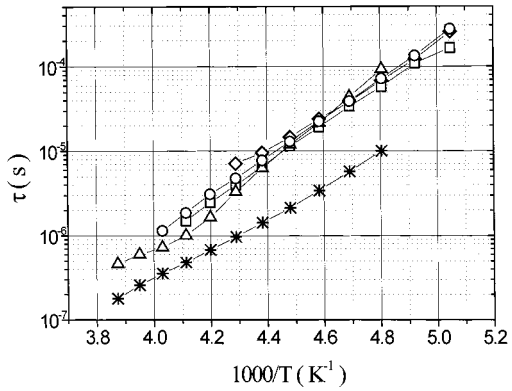

Figure 2. Temperature dependence of the characteristic relaxation times of the first relaxation process for samples 60 (*), 70 (◇), 80 (□), 90 (△), and 100 (○).

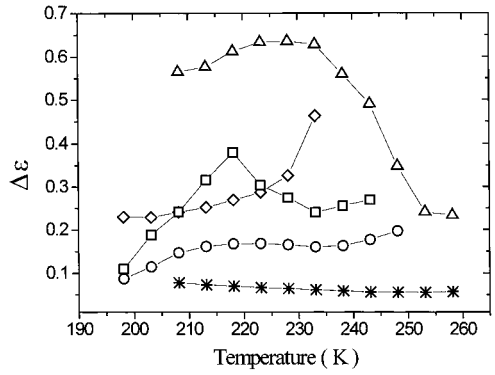

Figure 3. Temperature dependence of the dielectric strength of the first relaxation process for samples 60 (*), 70 (◇), 80 (□), 90 (△), and 100 (○).

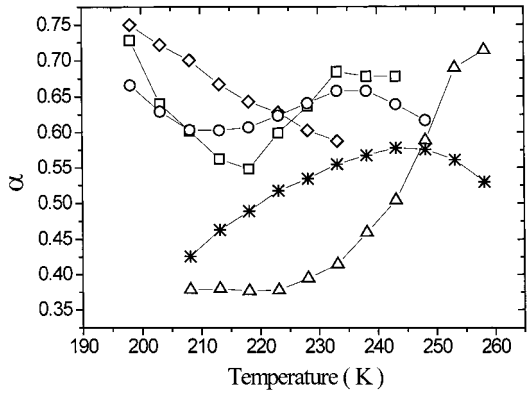

Figure 4. Temperature dependence of the stretched parameter α of the first relaxation process for samples 60 (*), 70 (◇), 80 (□), 90 (△), and 100 (○).

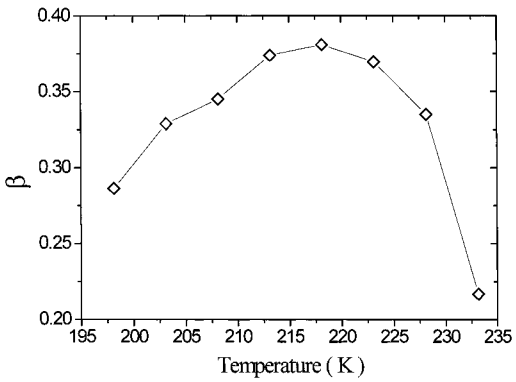

Figure 5. Temperature dependence of the stretched parameter β of the first relaxation process for sample 70.

typical view of the 3-D plot of dielectric losses vs frequency and temperature is shown in parts a and b of Figure 1 for two edging samples 100 and 60. One can see that the complex non-Debye dielectric behavior can be described in terms of few distributed relaxation processes.

The first relaxation process is well marked for all the samples at the temperature interval −80 to +10 °C. This process we associate with the dynamics of the mobile molecules and ions interacting with the pore surface. The temperature dependencies of the HN fitting parameters τ_1, $\Delta\epsilon_1$, α_1, and β_1 of the first process are presented in Figures 2−5. The dependencies of the relaxation times versus temperature for all the studied samples demonstrate an Arrhenius behavior with activation energies of 45 ± 10 kJ/mol (Figure 2) and correlate well with the activation energy of rearrangements of aggregates in acids.[15] Hence, the observed relaxation behavior can be related to the dissociation−association reaction of HCl molecules in the pores. These molecules may be anchored onto the multiple Si−O−Si bridges constructing the sol−gel porous matrix.

The dielectric strength reflects the morphology of the samples prepared at different temperatures. It is noteworthy that the dielectric polarization characterized by the dielectric strength has the highest magnitude for the first process in sample 90 and the smallest in sample 60 (Figure 3). Since the dielectric polarization depends on the amount of dipole-active species in each pore and since their concentration in the bulk is uniform, we assume that the dielectric strength correlates with the size of the larger the ladder-segment-derived pores. Therefore, we can attribute these findings to the existence of the largest ladder-segment-derived pores in sample 90 and the smallest in sample 60. These results are in accord with the mechanical flexibility of samples 80−100, compared with the rigidity and fragility of sample 60 cracking during drying. The temperature behavior of the fitting HN parameters α_1 and β_1 also reflects the dependence of material morphology on the preparation conditions. In fact, all the samples demonstrate the complex temperature behavior of parameter α_1 (Figure 4). In contrast, the parameter β_1 is practically 1 for samples 100, 90, 80, and 60 in the entire temperature range. In the case of sample 70, however, the parameter β_1 is much smaller than 1, demonstrating a complex temperature behavior (Figure 5). Such a behavior of the Havriliak−Negami parameters can be related to the variance of the morphology of pores and the short- and long-range interactions of HCl molecules with the pore surface and between themselves. This puzzling finding necessitates a further comprehensive analysis of the temperature behavior of many samples fabricated at different temperatures, as well as additional construction of the theoretical models, which are the subject of our ongoing research.

Figure 6 shows the typical behavior of the dielectric permittivity and dielectric losses at a fixed frequency as a function of temperature for all the samples investigated. The maximum of dielectric permittivity is located around 30−40 °C with a small deviation for sample 90. This maximum is hardly observed for sample 60, which undergoes heavy fragmentation upon drying. In general, our observations during the synthesis of these materials teach us that the higher the fast sol−gel reaction temperature is, the more polymer-like the matrix behaves (and the less it is apt to undergo cracking). Contrarily, the lower the fast sol−gel reaction temperature is, the more particle-like the matrix behaves (and the more it undergoes cracking). The very

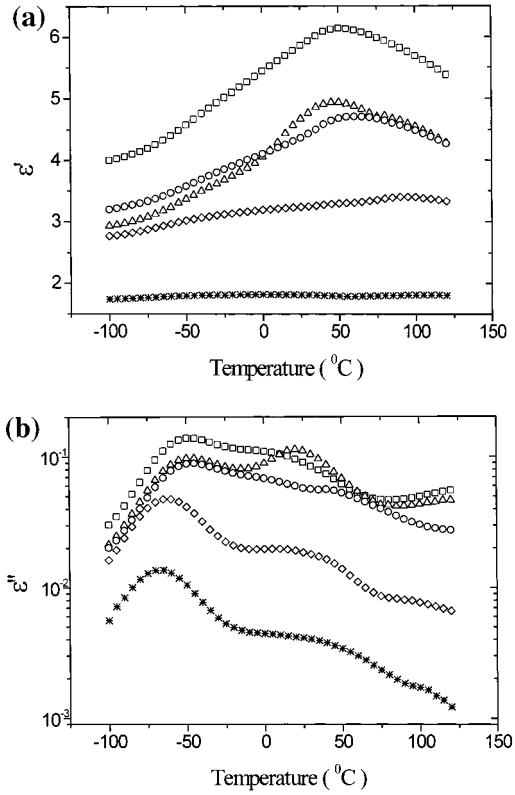

Figure 6. Temperature dependence of the low (8.65 kHz) frequency behavior of the dielectric permittivity ϵ' (a) and losses ϵ'' (b) for sol−gel samples 60 (*), 70 (◇), 80 (□), 90 (△), and 100 (○).

small intensity of the second peak in sample 60 can thus be attributed to extreme hydrophobic segregation of particles in the matrix.

Peaks on the curves of temperature dependencies of dielectric permittivity and dielectric losses in the temperature interval 30−40 °C correspond to the second relaxation process. The maxima of the dielectric permittivity curves have a very small temperature dependence. We note that such a behavior is typical for the percolation processes in glasses and microemulsions.[13,16] Thus, we can attribute this process to percolation of the electric excitation within the sol−gel derived fractal structure in the glass. The transport of the excitation is associated with mobility of the charge carriers within pores. The value of the dielectric permittivity depends on the rigidity of the polymer-like matrix and, therefore, on the mobility of charge carriers in the porous system.

Analysis of the dielectric relaxation parameters of the percolation process in the time domain allows us to determine the geometrical characteristics of the porous medium. The dielectric response for this process can be described by Kohlrausch−Williams−Watts (KWW) expression $\Psi(t/\tau) \approx \exp(-(t/\tau)^{\nu})$, where Ψ is the dipole correlation function (DCF), τ is the average relaxation time, and ν is the stretched parameter, $0 < \nu \leq 1$. It was shown[17] that in complex fractal systems, for the relaxation related to the transfer of the electric excitation along the ramified path, the stretched parameter ν can be related to the fractal dimension D_f of the path, $\nu = D_f/3$. We assume that the fractal dimension of this pass coincides with the fractal dimension of the pore space.

To describe the porous medium, the relationship between the fractal dimension and porosity of the material was obtained by using the model of random fractal.[18,19] In the simplest case of the model, the mean deviations of the scaling parameters of the random fractal from the scaling parameters of the regular

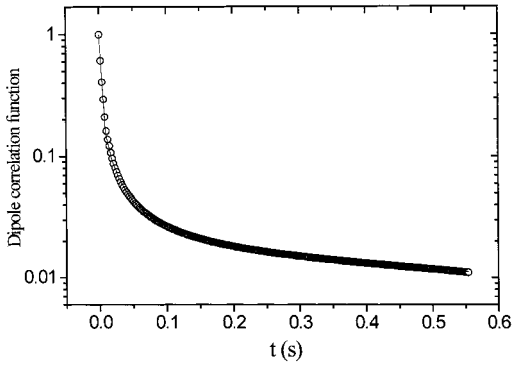

Figure 7. Macroscopic dipole correlation function of sample 100 at the temperature corresponding to the second relaxation process. The solid line corresponds to a fit of the KWW equation to the data.

TABLE 1: Values of Fractal Dimension and Porosity for Samples 100, 90, 80, and 70

sol−gel preparation temp (°C)	fractal dimension D_f	porosity ϕ from specific gravity (%)	porosity ϕ from dielectric measurements (%)
100	0.87	30	32
90	1.53		40
80	0.82		31
70	0.74		31

dominating fractal are zero. This makes it possible to obtain the approximate relationship between the porosity ϕ and the fractal dimension D_f of the porous space:

$$\phi = \frac{1}{4 - D_f} \frac{1 - \mu^{4-D_f}}{1 - \mu} \approx \frac{1}{4 - D_f} \tag{4}$$

where $\mu = \lambda/\Lambda$, λ is the minimal scale (∼pore size), Λ is the maximal scale (∼sample size).

The experimental macroscopic dipole correlation functions for samples 100, 90, 80, and 70 at the temperature corresponding to the second process, respectively, have been obtained by an inverse Fourier transform. The complex dielectric permittivity expressed in terms of the DCF is given by

$$\epsilon^*(\omega,T) = \epsilon_\infty - (\epsilon_s - \epsilon_\infty)\hat{F}\left(\frac{d}{dt}\Psi(t)\right) \tag{5}$$

where $\hat{F}$ is the operator of the Fourier transform and the parameters ϵ_s and ϵ_∞ are the static dielectric permittivity and its high-frequency limit, respectively. A typical behavior of the DCF versus the time, obtained from the low-frequency dependence of the dielectric permittivity at the percolation temperature, is shown in Figure 7.

The DCF displays a complex nonexponential time behavior that can be deconvoluted at the temperature and corresponds to percolation into the sum of two KWW processes. The short relaxation time is related to the first relaxation process at this temperature, while the long time process is associated with the percolation process. This long time behavior of the DCF have been fitted to KWW relationship with the purpose of determining the stretched parameter ν, which was used for the calculation of fractal dimension D_f of the samples. The values of fractal dimension and porosity of the samples are shown in Table 1. Fractal dimensions D_f obtained for samples 100, 80, and 70 are smaller than 1. Such small values of the fractal dimensions indicate that the pores are rather discrete (plausibly, blocked pores) than interconnected. The fractal dimension of sample 90 is larger than 1. This value can be explained in terms of the

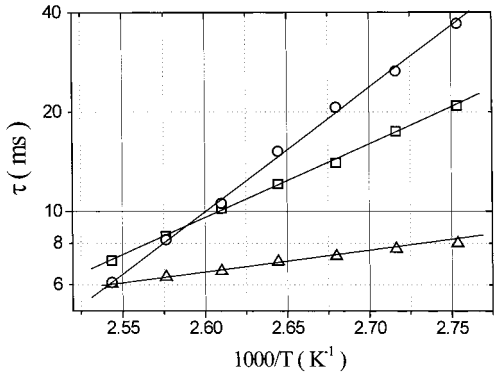

Figure 8. Temperature dependence of the characteristic relaxation times of the high-temperature transition for the various samples. The solid lines are a fit of the Arrhenius equation to the data.

transfer of electric excitation along the surface of interconnected pores.[19] Such pore interconnection can be attributed to a larger value of the average size of pores in this sample. The larger value of the average pore size indicates a larger length of linear chain segments formed at this specific temperature, or in other words, a smaller density of interchain junctions (cross-links), where isolated hydroxy groups may remain and, hence, hydrophilic moieties may be formed.

We compared the value of porosity obtained from eq 4 with that measured for sample 100 by the specific gravity method. The value obtained from dielectric spectroscopy measurements ($\phi \approx 0.32$) is in a very good agreement with the data ($\phi \approx 0.30$) obtained from independent measurement.

In the temperature region above 60 °C at the low-frequency band, materials 80, 90, and 100 appear slightly electrically conductive and show an increase of the dielectric losses in the low-frequency limit. Samples 60 and 70, in which the sol−gel reaction took place at lower temperatures, do not display such increase on the relaxation spectra. To analyze the nature of the relaxation in this temperature region, we need first to subtract the dc conductivity contribution from the spectrum. An Arrhenius plot for the third process relaxation time in samples 80, 90, and 100 has been drawn after the subtraction of the conductivity (Figure 8). The activation energies calculated for samples 80, 90, and 100 are 47, 13, and 76 kJ/mol, respectively. Sample 90 demonstrates the shortest relaxation times and rather small magnitude of the activation energy, which may be associated with the fast mobility of the terminal oxygen groups.[20] The relatively high activation energy for samples 80 and 100 seems to be attributed to the local molecular mobility of the chain fragments located between neighboring knots of the entangled three-dimensional network.[21] The difference in the activation energy amplitudes for these samples can be due to the different density of cross-links formed as a result of sol−gel formation.

4. Conclusions

The dielectric response of porous sol−gel glasses prepared via the fast sol−gel route is sensitive to the morphology changes of sol−gel samples depending on the preparation temperature, which affects the kinetics of all chemical processes involved. The dielectric relaxation has a complex nonexponential behavior with some common features for all the studied matrices. It is associated with the complex dynamics of hydrochloric acid (HCl) molecules and ions and reflects their interactions with the pore surface. The dielectric spectrum can be represented as a sum of three non-Debye relaxation processes and conductivity. Analysis of the dielectric spectra enables us to calculate the fractal dimension, D_f, and the material porosity, ϕ, of samples. Finally, the intriguing coexistence of two relaxation processes, one typical of glasses and one typical of polymer, is in accord with the dual behavior of the fast sol−gel derived matrices and in accord with their chemical constitution, an "average" of quartz and silicon rubber.

Acknowledgment. We express our appreciation to Dr. Alexander Puzenko for helpful discussions. The authors express their gratitude for the financial support of this research by Israel Ministry of Science and the Arts, Grant 8559-1-95.

References and Notes

(1) Brinker, C. J.; Scherer, G. W. *Sol−Gel Science: The Physics and Chemistry of Sol−Gel Processing*; Academic Press: San-Diego, CA, 1990.
(2) Haruvy, Y.; Webber, S. E. *Chem. Mater.* **1991**, *3*, 501.
(3) Haruvy, Y.; Webber, S. E. Fast Sol−Gel Preparation of Glasses, U.S. Patent 5,272,240, 1993.
(4) Haruvy, Y.; Heller, A.; Webber, S. E. Sol−Gel Preparation of Optically Clear Supported Thin-Film Glasses Embodying Laser Dyes−Novel Fast Method. In *Supramolecular Architecture: Synthetic Control in Thin Films and Solids*; Bein, T., Ed.; Proceedings of the ACS Symposium 499; American Chemical Society: Washington, DC, 1992; Chapter 28.
(5) Haruvy, Y.; Webber, S. E. *Mater. Res. Symp. Proc.* **1992,** *271*, 297.
(6) Haruvy, Y.; Gilath, I.; Manewictz, M.; Eisenberg, N. *Chem. Mater.* **1997**, *9*, 2604 (special issue on sol−gel derived materials).
(7) Mackenzie, J. D., Ed. *Sol−gel optics II*; Proceedings of SPIE, July 20−22, 1992, San Diego, CA; SPIE: Bellingham, WA, 1992; p 1758.
(8) Lebeau, B.; Maquet, J.; Sanches, C.; Toussaere, E.; Hierle, R.; Zyss, J. *J. Mater. Chem.* **1994**, *4*, 1855.
(9) Chambers, R. C.; Jones, W. E., Jr.; Haruvy, Y.; Webber, S. E.; Fox, M. A. *Chem. Mater.* **1993**, *5*, 1481.
(10) Hibben, Q.; Lu, E.; Haruvy, Y.; Webber, S. E. *Chem. Mater.* **1994**, *6*, 761.
(11) Chemla, D. S.; Zyss, J. *Nonlinear Optical Properties of Organic Molecules and Crystals*; Academic Press: New York, 1987.
(12) Zyss, J., Ed. *Molecular Nonlinear Optics*; Academic Press: New York, 1994.
(13) Gutina, A.; Axelrod, E.; Puzenko, A.; Rysiakiewicz-Pasek, E.; Kozlovich, N.; Feldman, Yu. *J. Non-Cryst. Solids* **1998**, *235−237*, 302.
(14) Schaumburg, G. Dielectrics Newsletter, November 1997.
(15) Shahparonov, M. I.; Kasimhodzhaev, P. S.; Levin, V. V.; Lupina, M. I. *Physics and Physical Chemistry of Liquids*, 2nd ed.; Moscow University, 1973.
(16) Feldman, Yu.; Kozlovich, N.; Nir, I.; Garti, N. *Phys. Rev. E* **1995**, *51*, 478.
(17) Feldman, Yu.; Kozlovich, N.; Alexandrov, Yu.; Nigmatullin, R.; Ryabov, Ya. *Phys. Rev. E* **1996**, *54*, 5420.
(18) Nigmatullin, R. R. *Phys. Status Solidi. B* **1989**, *49*, 153.
(19) Puzenko, A.; Kozlovich, N.; Gutina, A.; Feldman, Yu. *Phys. Rev. B*, submitted.
(20) Hedvig, P. *Dielectric Spectroscopy of Polymers*; Adam Hilger, Ltd.: Bristol, 1977.
(21) Sperling, L. H. *Interpentrting Polymer Networks and Related Materials*; Plenum: New York, 1981.